John von Neumann Institute for Computing

Twisted Coronal Magnetic Loops and the Kink Instability in Solar Eruptions

Tibor Török, Bernhard Kliem

published in

NIC Symposium 2004, Proceedings,
Dietrich Wolf, Gernot Münster, Manfred Kremer (Editors),
John von Neumann Institute for Computing, Jülich,
NIC Series, Vol. **20**, ISBN 3-00-012372-5, pp. 25-36, 2003.

http://www.fz-juelich.de/nic-series/volume20

Twisted Coronal Magnetic Loops and the Kink Instability in Solar Eruptions

Tibor Török[1,2] **and Bernhard Kliem**[1]

[1] Astrophysical Institute Potsdam, 14482 Potsdam, Germany
[2] Institute of Mathematics, University of St Andrews, St Andrews, Fife KY16 9SS, UK
E-mail: {*ttoeroek, bkliem*}*@aip.de*

An instability of twisted magnetic flux tubes in the solar corona is regarded as a possible initiation process of solar eruptions. We study the stability properties and the dynamic evolution of such coronal magnetic loops using 3D numerical simulations within the framework of ideal (non-resistive) magnetohydrodynamics (MHD). Two different loop models are considered. First, an initially potential magnetic flux bundle is twisted continuously by small-scale vortex motions centred at its photospheric footpoints. A twisted flux tube is formed which starts to evolve quasi-statically along a sequence of force-free equilibria. During this phase, the flux tube ascends very slowly, similar to observed pre-eruption behaviour. There exists a critical twist beyond which no equilibrium can be found in the simulations and the flux tube ascends rapidly. It develops a helical shape during the rise, which indicates that the kink instability occurs. We follow the rise up to a height of ~ 3 solar radii, i.e., into the acceleration region of the solar wind. Hence, on the Sun the rapid rise of the flux tube would be observed as an eruption. Second, the analytical force-free coronal loop model by Titov and Démoulin[1] is used as the initial condition in the simulations. The amount of twist within the loop is a parameter that can be freely chosen so that a more systematic study of the kink instability becomes possible. This loop model is clearly found to be kink-unstable if a critical twist is exceeded. The growing kink perturbation leads to the formation of current sheets, which steepen exponentially and define the locations of plasma heating. Due to the twist in the magnetic field, the heated structures are S shaped – in very good agreement with soft X-ray observations of solar eruptions. This model, however, does not yet show a successful eruption, rather the kink instability starts to saturate. We discuss two improvements of the model which are promising with regard to eruption: a modification of the equilibrium so that the surrounding magnetic field decreases more rapidly with height and the inclusion of magnetic reconnection in a resistive MHD description.

1 Introduction

Large-scale solar eruptive events like flares, eruptive prominences, and coronal mass ejections (CMEs) are the most violent energy release processes in our solar system. They occur in the coronal layers of the solar atmosphere and preferentially in the active regions formed by sunspot groups, i.e., mainly at the maxima of the solar activity cycle. The time-scale of such events is within the range of minutes up to several hours and the length-scale is comparable to the sunspot distance but can finally exceed the size of the Sun (Fig. 1). During the largest solar eruptions, more than ten billion tons of solar plasma are ejected into the interplanetary space and particles are accelerated to energies of up to ~ 20 GeV. These particles are sufficiently energetic to destroy satellites and to harm astronauts seriously. Furthermore, disturbances of the geomagnetic field caused by solar eruptions are able to disrupt ground communications and power grids. Understanding the physics behind solar eruptions, a prerequisite to forecasting, is therefore of broad significance. The effects of solar eruptions on the Earth are considered within the new field of research referred to as Space Weather[3].

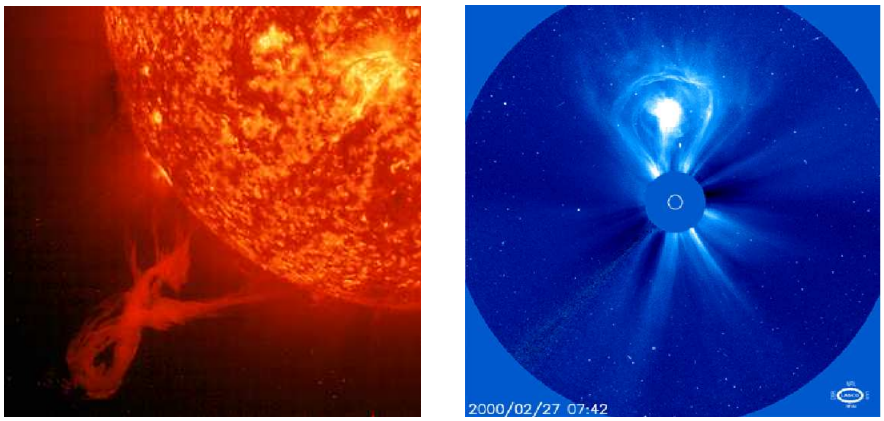

Figure 1. Solar eruptions observed by different instruments onboard the SOHO [2] satellite during the latest solar maximum. *Left:* eruptive prominence as seen by the EIT telescope in extreme ultraviolet light. *Right:* CME as seen by the LASCO/C3 coronagraph. The solar surface (indicated by the white circle) is covered by an occulting disc in order to allow the observation of regions of enhanced coronal density in the scattered white light.

Since the magnetic energy dominates all other forms of energy in the solar corona, there is general consensus that solar eruptions must be primarily magnetically driven[4]. However, their initiation process as well as their dynamic evolution are still poorely understood. The most commonly accepted models of solar eruptions ("storage and release models") assume that the energy released during the eruption is stored in the coronal magnetic field prior to the eruption, and that a loss of stability, or even a "loss of equilibrium" (a catastrophe) of the magnetic configuration leads to the eruption and energy release. Since the coronal magnetic field is observed to be generally very nearly force free, $\nabla \times \mathbf{B} = \alpha(\mathbf{x})\mathbf{B}$, and in equilibrium, the necessary energy for solar eruptions must be accumulated during a slow, quasi-static evolution on time-scales of hours to days. It is believed that slow motions at the solar surface (photosphere) or emerging new magnetic flux from the solar interior (convection zone) transfer energy into the corona by stressing the coronal magnetic field lines which are anchored in these layers. Eventually, these stresses exceed a threshold beyond which a stable equilibrium does not exist, and the coronal field erupts. In these models, arcade-like or flux-rope-like magnetic fields are typically chosen as initial coronal configurations, with dipolar or quadrupolar photospheric field distributions, and shearing, twisting, or converging motions are considered as driving photospheric motions[4,5].

Solar eruptions often show the phenomenology of a loop-shaped magnetic flux system with fixed footpoints at the coronal base and signatures of magnetic twist (Fig. 1). A single twisted magnetic flux tube appears to contain essential elements of the magnetic topology of the unstable erupting flux. The canonical instability of a twisted magnetic flux tube is the kink instability. A small perturbation of a kink-unstable flux tube leads to an exponentially growing helical distortion ("kink") of the tube. The simplifying assumption of straight, cylindrically symmetric flux tube equilibria has been used in all previous investigations of the kink instability for conditions appropriate to the solar corona[6]. The instability occurs if the twist, $\Phi(r) = lB_\phi(r)/(rB_z(r))$, exceeds a critical value, Φ_c. Here l is the length of the cylinder, r is the radial coordinate, and B_z and B_ϕ are the axial and azimuthal field

components, respectively. The twist equals 2π times the number of windings of the field lines around the loop axis. In most configurations of practical interest it depends on r and a critical average twist is then determined. The threshold for the onset of the instability depends on the details of the considered equilibrium, in particular on the radial profile, $\Phi(r)$, and on the aspect ratio, l/a, where a is the characteristic radius of the configuration (the minor radius in a toroidal system). For a straight, cylindrically symmetric flux tube with fixed (line-tied) ends and uniform twist (the Gold-Hoyle force-free equilibrium[7]), which is the simplest possible model of a coronal loop, the threshold was numerically determined[8] to be $\Phi_{\rm c} \approx 2.49\pi$.

This paper gives a summary of our ongoing studies[9–11] of the stability properties and the dynamic evolution of arched twisted magnetic flux tubes. The simulations are directed at the question whether coronal loops become unstable if they are sufficiently twisted and whether such an instability can lead to an eruption of the configuration. Two different approaches are considered.

First, an initially potential magnetic flux bundle is twisted continuously by photospheric vortex motions centred at the areas of the highest flux concentration. This configuration is a simple model of an active region on the Sun containing two rotating sunspots which are connected by bundles of magnetic field lines. The vortex motions form a twisted loop-shaped flux tube and possibly drive it towards instability and eruption. Indications supporting this conjecture were first obtained by Amari et al[12]. Our simulations confirm their results using different numerical tools, and relate the eruption to the occurrence of the kink instability, but we also find that the photospheric vortices influence a large volume around the unstable loop, which motivates us to study twisted loops that are not associated with driving motions at the boundary of the considered domain.

The analytical coronal magnetic loop model recently developed by Titov and Démoulin (T&D)[1] offers the possibility to perform the first stability analysis of an arched twisted flux rope free from driving at a boundary. This approximate force-free equilibrium contains an already twisted and curved current-carrying flux tube. The amount of magnetic twist in this model is a parameter that can be freely chosen. For small amounts of twist, we show that the analytical configuration is very close to a stable numerically obtained equilibrium. If a critical twist is exceeded, the loop is always found to be kink-unstable. The kink mode with rising loop apex forms structures that are in excellent agreement with X-ray observations of solar eruptions. On the other hand, we have not yet been able to find an eruption of the loop in our simulations, rather the very strong surrounding magnetic field in the T&D model eventually slows down the rise of the loop. First tests indicate, however, that a modified T&D model with a more realistic surrounding field and the inclusion of magnetic reconnecion by proceeding to resistive MHD simulations can both permit a full eruption of the twisted loop.

On the Sun, the situation is presumably in between our two models, with much of the twist already contained in the flux that emerges from the interior into the corona but a broad spectrum of twisting, shearing or converging motions always being present. Combined studies like the ones presented here will help single out the important effects that cause solar eruptions.

2 Numerical Model

We integrate the compressible ideal one-fluid MHD equations given by the continuity equation, the momentum equation, the induction equation (which follows from Ohm's law), Ampere's law for the current density, and an energy equation as follows

$$\partial_t \rho = -\nabla \cdot (\rho\, \mathbf{u})\,, \tag{1}$$

$$\rho\, \partial_t \mathbf{u} = -\rho\, (\, \mathbf{u} \cdot \nabla\,)\, \mathbf{u} + \mathbf{j} \times \mathbf{B} - \nabla\, \mathbf{p} + \nabla \cdot \mathsf{T}\,, \tag{2}$$

$$\partial_t \mathbf{B} = \nabla \times (\, \mathbf{u} \times \mathbf{B}\,)\,, \tag{3}$$

$$\mathbf{j} = \mu_0^{-1} \nabla \times \mathbf{B}\,, \tag{4}$$

$$\partial_t U = -\nabla \cdot \mathbf{S}\,. \tag{5}$$

Here $\mathbf{B}$, $\mathbf{u}$, ρ, p, $\mathbf{j}$, U, $\mathbf{S}$, and T are the magnetic field, velocity, mass density, pressure, current density, total energy density, energy flux vector, and viscous stress tensor, respectively. The latter are defined by

$$U = \rho\, w + \frac{\rho}{2}\, u^2 + \frac{B^2}{2\, \mu_0}\,,$$

$$\mathbf{S} = (\, U + p + \frac{B^2}{2\, \mu_0}\,) \mathbf{u} - (\mathbf{u} \cdot \mathbf{B}) \frac{\mathbf{B}}{\mu_0}\,,$$

$$\mathsf{T}_{ij} = \rho\, \nu\, \left(\frac{\partial u_i}{\partial x_j} + \frac{\partial u_j}{\partial x_i} - \frac{2}{3}\, \delta_{ij}\, \nabla \cdot \mathbf{u} \right)\,,$$

where w is the internal energy per unit mass and ν is the kinematic viscosity. The system is closed by an adiabatic equation of state, $p = (\, \gamma - 1\,)\, \rho\, w$, which is appropriate for the nearly collisionless corona. The ratio of specific heats is $\gamma = 5/3$. Viscosity is included only to improve the numerical stability and to facilitate relaxation towards equilibrium for the stable configurations.

The system of equations has been simplified for most of the calculations presented here by adopting the zero-beta assumption. The plasma-beta, $\beta = p/(B^2/2\mu_0)$, is of order $10^{-3} \ldots 10^{-2}$ in the inner solar corona where the eruptions are initiated. This eliminates the pressure in Eq. (2) and decouples the energy equation from the system. In order to investigate the scaling of kink mode growth rates with the plasma-beta, some runs were perfomed with the full system of equations.

We use a standard normalization of the variables. Lengths, velocities and times are normalized, respectively, by a characteristic length of the initial configuration, Λ (e.g., the half-distance between the footpoints of the flux rope [sunspots]), the initial maximum Alfvén velocity, $v_{\mathrm{a}0} = B_0^2/(\mu_0/\rho_0)^{1/2}$, and the corresponding Alfvén time $\tau_{\mathrm{a}} = \Lambda/v_{\mathrm{a}0}$. Here B_0 is a characteristic field strength, it is chosen to be the normal field component at

	L_x	L_y	L_z	$\Delta_{\min}$	$\Delta x_{\max}$	$\Delta y_{\max}$	$\Delta z_{\max}$	grid points
Sect. 3	100	100	200	0.03	9	9	12	$195 \times 165 \times 150$
Sect. 4	5	5	10	0.02	0.4	0.4	0.8	$141 \times 160 \times 200$

Table 1. Parameters of the numerical grids used in Sects. 3 and 4.

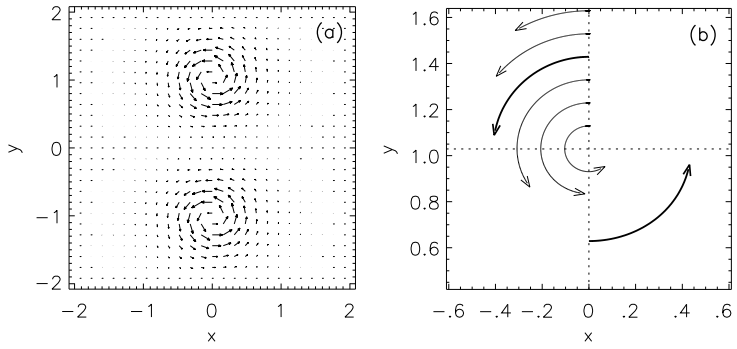

Figure 2. (*a*) Imposed velocity field. (*b*) Paths of fluid elements in the upper vortex with a peak velocity of $v_0 = 10^{-2} v_{\rm a0}$ after $75\tau_{\rm a}$, which corresponds to a twist in the formed central flux tube of $\Phi_{\rm g} \approx 2.5\pi$. The thick arrows indicate the positions where the outer (blue) and inner (green) flux bundles in Fig. 3 start from.

the loop footpoints in our externally driven system and the total field on the loop axis for the T&D equilibrium. For further details of the normalization, see Ref. 9.

As the physical domain we consider a finite cube of size $[-L_x, L_x]\times[-L_y, L_y]\times[0, L_z]$. Since the considered configurations possess line symmetry with respect to the z axis and since this symmetry is preserved throughout their evolution, the simulation domain can be restricted to the "half cube" $[-L_x, L_x]\times[0, L_y]\times[0, L_z]$. Inside this area, the equations are discretized on a nonuniform Cartesian grid. The grid spacing increases exponentially from a minimum value $\Delta_{\rm min}$ in the vicinity of the origin to maximum values $\Delta x_{\rm max}$, $\Delta y_{\rm max}$, and $\Delta z_{\rm max}$ at the outer boundaries. The grid parameters used in the simulations are given in Tab. 1. Grids of this size require the use of vector computers such as the CRAY SV1.

Eqs. (1)–(3) are rewritten in a flux conserving form, $\partial_t \mathbf{U} + \partial_x \mathbf{F}(\mathbf{U}) + \partial_y \mathbf{G}(\mathbf{U}) + \partial_z \mathbf{H}(\mathbf{U}) = 0$, where $\mathbf{U} = (\rho, \rho\, u_x, \rho\, u_y, \rho\, u_z, B_x, B_y, B_z)$ is the vector of the integration variables and $\mathbf{F}$, $\mathbf{G}$, and $\mathbf{H}$ are nonlinear flux terms[13]. A modified two-step Lax-Wendroff-method, adapted from Ref. 13, is employed for the numerical integration[9]. A variable time step is used according to the Courant-Friedrichs-Lewy stability criterion. The stability of the numerical scheme is further improved by applying artificial smoothing[14] to selected variables after each integration step in addition to the stabilization by the viscosity[9]. Closed boundary conditions are used at all boundaries, except at the front plane $\{y = 0\}$, where the variables are mirrored according to the line symmetry. In the cases with imposed vortex motions at the bottom plane $\{z = 0\}$, the tangential components of the magnetic field at the bottom boundary are obtained by extrapolation.

3 The Evolution of Twisting Coronal Magnetic Flux Tubes

We start with a potential, i.e., current-free and hence stable equilibrium field, which is created by two vertical, oppositely directed dipoles. The dipoles have a typical distance of 2 ($\sim$ 70 Mm) and are placed sufficiently below the photospheric layer $\{z = 0\}$ to obtain a realistic field distribution in $\{z = 0\}$. The initial density is set to $\rho_0 = B_0^2$ so that the initial Alfvén velocity $v_{\rm a0} = 1$ ($\sim 1000\,{\rm km\,s^{-1}}$) is uniform. Twist is continuously injected

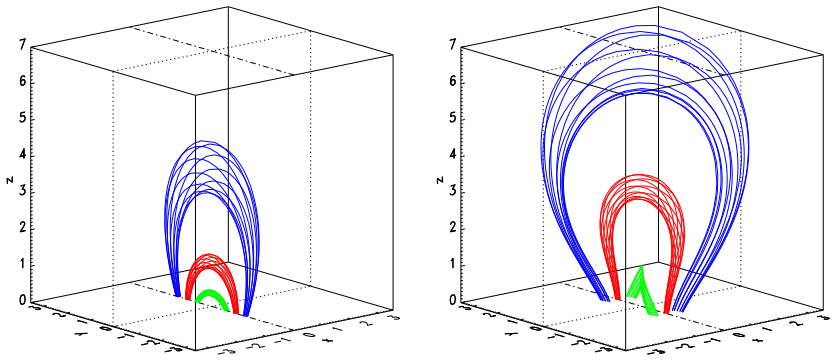

Figure 3. Evolution of selected magnetic field lines. The red lines show the twisted flux tube. The start regions of the green and blue field lines in the right-hand plot are marked by the heavy arrows in Fig 2b. The field lines are shown at the beginning of the simulation (*left*) and before the onset of eruption at a twist $\Phi_{\rm g} \approx 2.5\pi$ (*right*).

by prescribed vortex motions in $\{z = 0\}$, centered at the photospheric flux concentrations, see Fig. 2. The peak velocity in the photospheric vortices must be much smaller than the characteristic coronal MHD velocity, $v_0 = (10^{-3} \ldots 10^{-2}) v_{\rm a0}$. We use the condition $\beta = 0$ in these simulations.

3.1 Quasi-Static Evolution

As the vortices are switched on, the volume permeated by the magnetic field lines which are rooted in the area of the vortices starts to expand in all directions (Fig. 3). Field lines starting in the vicinity of the vortex centres form a central twisted flux tube which ascends and expands also laterally. The surrounding field lines are less twisted but sheared by the enforced differential rotation. All field lines develop helical shape, their photospheric projection is either S shaped or inverse-S shaped, as is often the case for magnetic loops in solar active regions.

Initially, the rise velocity of the twisted flux tube stays small, $|\mathbf{u}| \ll v_{\rm a}$, of the order of the driving velocity in the bottom plane. The flux tube stays nearly force free and, hence, evolves quasi-statically through a sequence of equilibrium states in this phase, as required for storage-and-release models of solar eruptions. This is confirmed by relaxation runs that are started from twisted states and have the vortices switched off: a relaxed state very close to the starting state is always obtained (Fig. 4, *left*).

3.2 Dynamic Expansion and Eruption

The evolution of the system changes fundamentally as soon as the accumulated twist of the central flux tube exceeds a critical value, $\Phi_{\rm c}$. The flux tube is then rapidly accelerated to near Alfvén velocity. None of our relaxation runs led to a new stable equilibrium, rather, the fast rise of the flux tube continued during the relaxation attempt as far as it could be followed, for $\sim 10^3\ \tau_{\rm a}$ to a height of $\sim 3\ R_\odot$. Such heights are within, probably already beyond the acceleration region of the solar wind (which is not yet included in our simulation model), so that on the Sun the flux tube would continue its fast rise and the process would be observed as an eruption (Fig. 1, *right*).

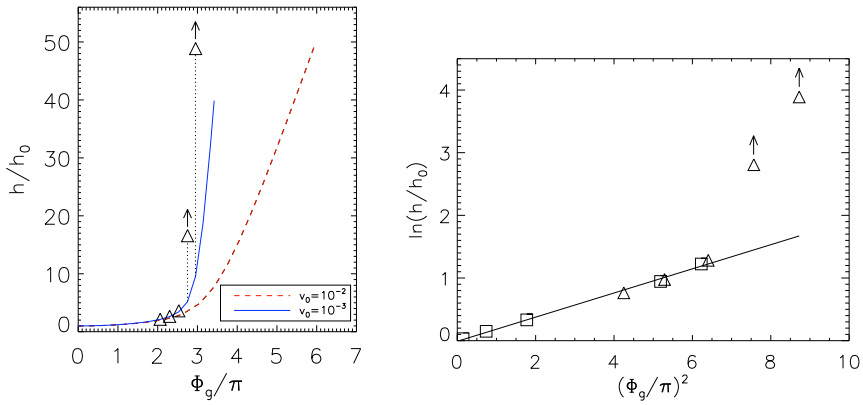

Figure 4. *Left:* apex heights of the flux tube as a function of twist for runs with different driving velocities. Triangles show heights at the end of relaxation runs for states calculated from the run with $v_0 = 10^{-3}$; the final two datapoints show still rising states, which were not relaxed at termination of the runs (see text). The initial apex height is $h_0 = 1.22$. *Right:* comparison of the apex heights after (or at termination of) relaxation with the rise characteristics $h \propto \exp(\mathrm{const} \cdot \Phi_g^2)$ of axially symmetric configurations from Sturrock et al[15]. Triangles are the same as in the left-hand plot, squares show relaxed states obtained from a run with a different initial density profile, $\rho_0 = |\mathbf{B}_0|$, and $v_0 = 10^{-2}$ (see Ref. 9). A least-squares fit through the first eight datapoints is shown.

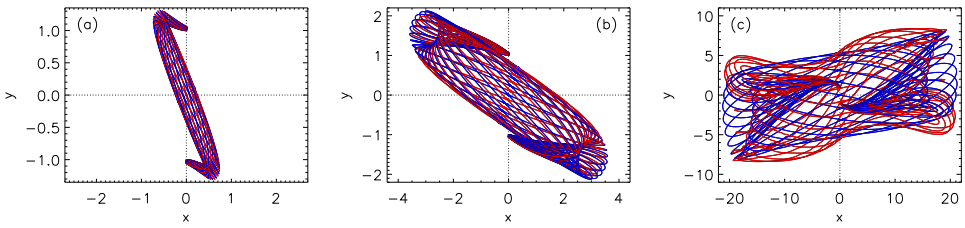

Figure 5. Field lines of the magnetic field (*blue*) and current density (*red*) in the central flux tube projected onto the bottom plane for $\rho_0 = B_0^2$ and $v_0 = 10^{-3}$. *(a)* Driven phase, $\Phi_g = 2.53\pi$ ($t = 721$). *(b)* Driven phase, $\Phi_g = 2.95\pi$ ($t = 841$; start of relaxation). *(c)* State at termination of the relaxation run at $\Phi_g = 2.95\pi$ ($t = 1785$). The huge expansion, helical distortion (kinking), and the deviation from force-freeness ($\mathbf{j} \not\parallel \mathbf{B}$) are obvious.

In Fig. 4 (*right*) we compare our numerical results with an analytical scaling of flux tubes heights in a simpler (axisymmetric) twisted configuration[15]. The agreement in the range of subcritical twists is nearly perfect, and it is clearly seen that the character of the evolution changes beyond a critical twist which for our system lies in the range $2.5\pi < \Phi_c < 2.75\pi$. Contrary to the conclusion made by Sturrock et al[15]. for their axisymmetric twisted configuration, and contrary to the well-known case of shearing arcade-like fields along the photospheric polarity inversion line[16], the opening of the initially closed field occurs for a *finite* amount of twist. Our critical twist is very close to the known threshold of the kink instability in a cylindrical configuration (Sect. 1), suggesting this instability as the cause for the loss of stable equilibrium. Indeed, the rising flux tube shows a strong helical distortion, which is characteristic of the ideal kink mode (Fig. 5).

The transition from quasi-static to dynamic eruptive evolution at a twist $\Phi_c \gtrsim 2.5\pi$ was found to be robust against variations of the dipole (sunspot) distance, vortex velocity, v_0, and density model, ρ_0. It confirms and extends the investigation by Amari et al.[12], who obtained a similar rapid rise of a sufficiently twisted flux tube for a different magnetic field model, $\mathbf{B}_0$. Further details of this study, such as indications for the formation of the three-part structure of CMEs, which consists of a dense core embedded in a cavity and an outer arc (Fig. 1, *right*), and the formation of S-shaped X-ray looops, can be found in Török and Kliem[9]. However, the obtained critical twist corresponds to a rotation of each sunspot by $\gtrsim 1.25\pi$, which exceeds observed rotations ($< 2/3\,\pi$) and suggests that part of the twist must already be present when the flux tube emerges through the photosphere. This leads us to investigate, in the following section, twisted flux tubes which do not have a large surrounding volume set into motion by photospheric vortices.

4 Kink Instability of Magnetic Loops and Sigmoid Formation

In this section we study the magnetic loop model by Titov and Démoulin[1] (Fig.6). This approximate, cylindrically symmetric, force-free equilibrium consists of a toroidal ring current of major radius R and minor radius a, whose outward-directed Lorentz self-force is balanced with the help of a field by two fictitious magnetic charges of opposite sign which are placed at the symmetry axis of the torus at distances $\pm L$ to the torus plane. That axis lies below the photospheric plane $\{z=0\}$ at a depth d. The resulting field outside the torus is current-free. A toroidal field component created by a fictitious line current running along the symmetry axis is added. Its strength controls the twist of the field in the torus, $\Phi_{\rm loop}$. The section in the volume $\{z > 0\}$ is a model of a coronal magnetic loop. The parameters of the model are chosen according to observed values of a typical active region on the Sun. The normalized geometrical parameters are $d = L = 1$ (50 Mm) and $R = 2.2$ and the twist is varied in the range (2–8)π. All boundaries of the physical domain are closed, no external stressing is applied to the system as it was the case in the simulations described in Sect. 3.

4.1 Parametric Study of the Ideal Kink Instability

For small values of the twist, the T&D loop model is found to be stable; the numerically obtained equilibrium is then always very close to the approximate analytical equilibrium. The kink instability clearly occurs if the critical twist is exceeded, which has a value of $\Phi_c \approx 3.5\pi$ for the particular set of parameters considered. The two principal cases of the instability, the downward and the upward kink of the loop apex, are shown in Fig. 7 for $\Phi_{\rm loop} = 4.9\pi$. For the given set of parameters, the downward kink develops spontaneously, while the upward kink is obtained by applying a small initial velocity perturbation at the loop apex. (This is reversed for some of the other parameter combinations studied.) See Török et al.[10] for a full parametric study of the kink instability growth rates, which also comprises the stabilizing effect of increasing $\beta \neq 0$.

The kink perturbation consists in a helical distortion of the loop. Accordingly, in both cases a helical current sheet wrapped around the loop is formed as the loop pushes into the surrounding field. This is analogous to the kink instability in straight (cylindrical) loop models. The upward kink perturbation additionally leads to the formation of a vertical

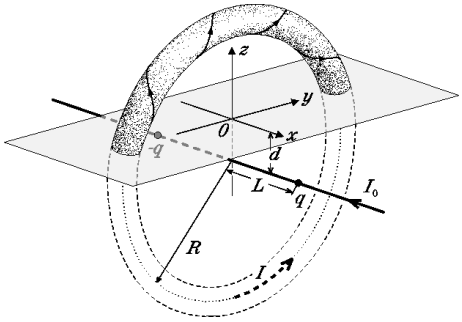

Figure 6. Schematic of the coronal magnetic loop model by Titov and Démoulin[1]. The plane $\{z = 0\}$ corresponds to the solar photosphere. The subphotospheric part has no physical significance.

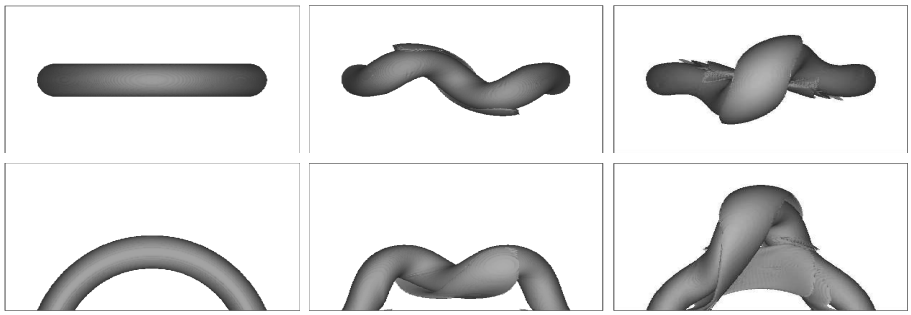

Figure 7. Top and side view on iso-surfaces of the current density at the beginning of the simulation (*left*) and after the development of the kink instability for the downward kinking case (*middle*) and for the upward kinking case (*right*), for a left-handed twist of 4.9π. The iso-surfaces outline the magnetic loop and the newly formed current sheets.

current sheet below the loop apex which has no counterpart in the cylindrical case. Such a vertical current sheet is the main hypothesis in the so-called standard model of solar eruptions[17]. In the T&D model, it is a natural consequence of the pinching of the hyperbolic field structure (a generalized X-type field line configuration) below the loop, which is trigged by the instability[10].

In the linear phase of the instability, the apex velocity, the current densities in the formed sheets, and the total kinetic energy in the box grow exponentially. In the nonlinear regime, however, the perturbations are slowed down by the strong magnetic field that surrounds the loop in the T&D model, and the instability starts to saturate without leading to a full eruption. Even this apparently unsatisfactory result is consistent with part of the observations: many flare events and some filament activations start with exponential characteristics but do not lead to escape of plasma from the Sun. Such an example is compared with our simulations in Fig. 8. We have begun to study a modified T&D equilibrium with a more rapidly decreasing surrounding field and have also included the resistive effect of magnetic reconnection in the formed current sheets. First results indicate that the kink instability of a twisted flux rope can lead to eruptive behaviour with features similar to those shown in Fig. 1.

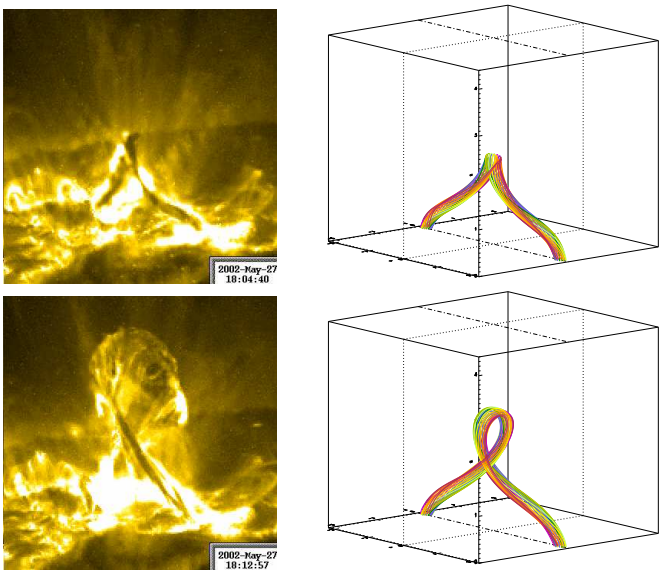

Figure 8. *Left:* two stages of a "failed" prominence eruption as observed by the TRACE[18] satellite in extreme ultraviolet light[19]. The lower image shows the prominence after its rise came to a stop. *Right:* field lines of the current density showing the unstable loop in the exponential rise phase (*upper plot*) and in the saturation phase (*lower plot*) of the kink instability.

4.2 Formation of Transient Sigmoids

Sigmoidal (S or inverse-S shaped) structures, which are suggestive of current-carrying, i.e., helical field lines, are often seen in soft X-ray images of solar active regions. A particularly bright and sharp form occurs transiently at the onset of eruptions. It is of practical relevance as an indicator for geoeffective eruptions. Sigmoids show a strong tendency to obey a "helicity rule": S shapes occur preferably in the southern solar hemisphere, where active regions possess preferably right-handed twist ($\alpha = \mathbf{j} \cdot \mathbf{B}/B^2 > 0$), and the inverse is true for the northern hemisphere, where the twist is preferably left-handed ($\alpha < 0$). There is a long-lasting debate whether sigmoids consist in kink-unstable loops[20] or whether they show so-called quasi-separatrix layers, i.e., layers in the magnetic field defined by a strong gradient of footpoint mapping of penetrating field lines, which are preferable locations of current sheet formation[1].

Our simulations show that upward kinking loops develop a sigmoidal photospheric projection that is opposite to the helicity rule (see Fig. 7 [*right*] which shows the S shape for a left-handed twist). This is a general property of the kink instability, in which the handedness of the perturbed loop axis equals the handedness of the field line twist. Figure 9 shows that the field lines passing through the vertical current sheet below the rising loop agree with the sense of observed sigmoids and reproduce many aspects of their detailed shape as well. This current sheet is formed at the hyperbolic flux tube made of two crossing quasi-separatrix layers[1]. See Török et al.[10] and Kliem et al.[11] for further details.

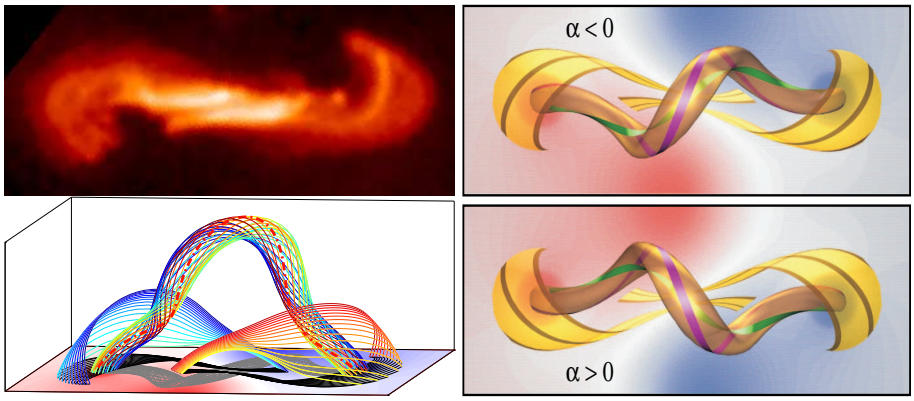

Figure 9. *Upper left*: transient sigmoid observed in an eruptive flare[21] which had primarily left-handed twist ($\alpha < 0$). *Lower left*: magnetic field lines of the configuration shown in the right panels of Fig. 7. One of the loop field lines is emphasized to indicate the left handedness of the twist. The field lines below the loop pass through two symmetrical vertical stripes close to the z axis that bracket the vertical curent sheet. The normal component of the magnetic field in the bottom plane (the "photospheric magnetogram") is shown color-coded (blue – positive, red – negative). Projections of the field lines are overlayed. *Right*: Top view on selected field lines and on the surfaces that they form. The field lines for $\alpha < 0$ are identical to those plotted in the lower left panel. The bottom panel shows similarly selected field lines of the system with reversed α at the same time.

5 Summary

The results presented here give an impression of the huge potential for 3D MHD simulations in modeling dynamic processes in magnetized astrophysical plasmas. The kink instability of twisted flux ropes was identified as a prime candidate for the initiation of solar eruptions, which are the main driver of the space weather. We have studied two systems in which either all of the twist was injected by driving at a boundary of the simulation domain (the photosphere) or all of the twist existed already in the initial configuration. Essential features of solar eruptions were reproduced so that the results can be used for diagnostic purposes in future applications, e.g., to estimate the twist of unstable flux that emerged from the convection zone. In general, a hybrid of our two idealized cases is to be expected on the Sun, which accounts for the great variety of phenomena observed in solar eruptions and requires more sophisticated modeling. Also, additional physical effects, in particular magnetic reconnection, should be included in future simulations.

Acknowledgments

The simulations presented here were performed on the Cray SV1 supercomputer of the John von Neumann-Institut für Computing, Jülich. The investigation was supported by BMBF/DLR grants No. 50 OC 9901 2 and 01 OC 9706 4, and by EU grant No. HPRN-CT-2000-00153.

References

1. V. S. Titov and P. Démoulin, *Basic topology of twisted magnetic configurations in solar flares*, Astron.&Astrophys. **351**, 707–720 (1999).
2. `http://sohowww.nascom.nasa.gov`.
3. J. L. Burch, R. L. Carovillano, and S. K. Antiochos (eds.), *Sun-Earth Plasma Connections*, Geophysical Monograph 109, AGU, Washington, 1999; see also `http://www.spaceweather.com`.
4. T. G. Forbes, *A review on the genesis of coronal mass ejections*, J. Geophys. Res. **105**, 23 153–23 165 (2000).
5. E. R. Priest and T. G. Forbes, *The magnetic nature of solar flares*, Astron.& Astrophys. Rev. **10**, 313–377 (2002).
6. A. W. Hood, *Instabilities in the solar corona*, Plasma Phys.& Contr. Fusion **34**, 411–442 (1992).
7. T. Gold and F. Hoyle, *On the origin of solar flares*, Monthly Not. RAS **120**, 89–105 (1960).
8. A. W. Hood and E. R. Priest, *Critical conditions for magnetic instabilities in force-free coronal loops*, Geophys. Astrophys. Fluid Dynamics **17**, 297–318 (1981).
9. T. Török and B. Kliem, *The evolution of twisting coronal magnetic flux tubes*, Astron.&Astrophys. **406**, 1043–1059 (2003).
10. T. Török, B. Kliem, and V. S. Titov, *Ideal kink instability of a magnetic loop equilibrium*, Astron.&Astrophys., submitted.
11. B. Kliem, V. S. Titov, and T. Török, *Formation of current sheets and sigmoidal structure by the kink instability of a magnetic loop*, Astron.&Astrophys., submitted.
12. T. Amari, J. F. Luciani, J. J. Aly, and M. Tagger, *Very Fast Opening of a Three-dimensional Twisted Magnetic Flux Tube*, Astrophys. J. **466**, L39–L42 (1996).
13. M. Ugai and T. Tsuda, *Magnetic field-line reconnexion by localized enhancement of resistivity. I - Evolution in a compressible MHD fluid*, J. Plasma Phys. **17**, 337–356 (1977).
14. T. Sato and T. Hayashi, *Externally driven magnetic reconnection and a powerful magnetic energy converter*, Phys. Fluids **22**, 1189–1202 (1979).
15. P. A. Sturrock, S. K. Antiochos, and G. Roumeliotis, *Asymptotic Analysis of Force-free Magnetic Fields of Cylindrical Symmetry*, Astrophys. J. **443**, 804–809 (1995).
16. P. A. Sturrock, *Plasma Physics*, Cambridge University Press 1994, Ch. 13.4–13.7.
17. K. Shibata, *Evidence of Magnetic Reconnection in Solar Flares and a Unified Model of Flares*, Astrophys. Space Sci. **264**, 129-144 (1999).
18. `http://vestige.lmsal.com/TRACE`.
19. H. Ji et al., *Observations of the Failed Eruption of a Filament*, Astrophys. J. **595**, L135–138 (2003).
20. D. M. Rust and A. Kumar, *Evidence for Helically Kinked Magnetic Flux Ropes in Solar Eruptions*, Astrophys. J. **464**, L199–L202 (1996).
21. P. K. Manoharan, L. van Driel-Gesztelyi, M. Pick, and P. Démoulin, *Evidence for Large-Scale Solar Magnetic Reconnection from Radio and X-Ray Measurements*, Astrophys. J. **468**, L73–L76 (1996).